fractal and fractional

MDPI

Article

Modelling of Electron and Thermal Transport in Quasi-Fractal Carbon Nitride Nanoribbons

Renat T. Sibatov [1,2,*], Alireza Khalili Golmankhaneh [3], Ruslan M. Meftakhutdinov [4] and Ekaterina V. Morozova [4] and Diana A. Timkaeva [4]

1 Moscow Institute of Physics and Technology (MIPT), Dolgoprudny 141700, Russia
2 Scientific-Manufacturing Complex "Technological Centre", Moscow 124498, Russia
3 Department of Physics, Urmia Branch, Islamic Azad University, Urmia 57169-63896, Iran; alirezakhalili2002@yahoo.co.in
4 Laboratory of Diffusion Processes, Ulyanovsk State University, Ulyanovsk 432017, Russia; postbox.mrm@gmail.com (R.M.M.); kat-valezhanina@yandex.ru (E.V.M.); dianatimkaeva@mail.ru (D.A.T.)
* Correspondence: ren_sib@bk.ru

Abstract: In this work, using calculations based on the density functional theory, molecular dynamics, non-equilibrium Green functions method, and Monte Carlo simulation, we study electronic and phonon transport in a device based on quasi-fractal carbon nitride nanoribbons with Sierpinski triangle blocks. Modifications of electronic and thermal conductance with increase in generation g of quasi-fractal segments are estimated. Introducing energetic disorder, we study hopping electron transport in the quasi-fractal nanoribbons by Monte Carlo simulation of a biased random walk with generalized Miller–Abrahams transfer rates. Calculated time dependencies of the mean square displacement bear evidence of transient anomalous diffusion. Variations of anomalous drift-diffusion parameters with localization radius, temperature, electric field intensity, and energy disorder level are estimated. The hopping in quasi-fractal nanoribbons can serve as an explicit physical implementation of the generalized comb model.

Keywords: quantum fractal; carbon nitride; density functional theory; anomalous diffusion; hopping; Monte Carlo simulation; comb model

Citation: Sibatov, R.T.; Golmankhaneh, A.K.; Meftakhutdinov, R.M.; Morozova, E.V.; Timkaeva, D.A. Modelling of Electron and Thermal Transport in Quasi-Fractal Carbon Nitride Nanoribbons. *Fractal Fract.* **2022**, *6*, 115. https://doi.org/10.3390/fractalfract6020115

Academic Editors: Ricardo Almeida and Trifce Sandev

Received: 7 December 2021
Accepted: 9 February 2022
Published: 15 February 2022

1. Introduction

The dimension of the electronic quantum system largely determines its properties. Particularly, in one-dimensional systems, electrons form the Luttinger liquid [1], and in two-dimensional systems, the quantum Hall effect is observed [2]. Little is known about the behavior of electrons in nanosystems of fractional dimension [3]. Recent works [3–5] on the synthesis of artificial molecular systems with quasi-fractal geometry provide new opportunities for experimental study of electronic properties in fractal atomic systems. The molecular quasi-fractal in the form of Sierpinski triangle was obtained in [5] by self-assembly of organic molecules by halogen bonds, hydrogen bonds, covalent bonds, and coordination interactions of metal–organic compounds on the surface. The resulting structure contains pores of different sizes in one triangular block and, according to forecasts in [5], it should have unique optical, magnetic, and mechanical properties.

In works [6–8], by means of the first principles calculations and semi-empirical methods, electronic properties of fractional-sized molecular systems were studied. In [8], quantum transport in the Sierpinski fractal triangles built on a graphene sheet is examined within the Hubbard model. Significant differences in the properties of structures with "zigzag" and "armchair" edges were found, similar to the situation with nanoribbons, quantum dots, or anti-dots. Sierpinski triangles with zigzag edges are characterized by a large proportion of boundary states which causes instability with respect to spin polarization. On the contrary, fractals with armchair edges remain balanced on spin. In both cases, the triangles are characterized by a large energy gap leading to pronounced optical absorption in the

visible range. It has been shown that the distribution of energy levels becomes self-similar for fractal sets of later generations. In [9], the authors suggested a fractal Kronig–Penney model describing the quantum behavior of a particle in a one-dimensional fractal lattice. In [10], the properties of plasmon transport in fractal Sierpinski carpets were experimentally examined. The observed mean squared displacements and the Polia numbers provided evidence for anomalous diffusion of plasmons in considered carpets. The authors of [10] related the critical point of transition from normal to anomalous transport with fractal geometry parameters.

Diffusion on fractals was actively studied in the 80–90s of the 20th century. In the case of quantum transport in fractal nanosystems, the wave nature of particles or quasiparticles (electrons, holes, phonons, excitons, etc.) is of decisive importance. In review [11], within the framework of the concept of fractons, the problems of propagation of elastic waves in fractal lattices and the problem of multiple scattering by fractal aggregates are considered. In these problems, the authors discover scale-invariant spectra of excitations of the medium observed during wave processes. A recent paper [12] proposes a fractal regularized long-wave equation describing waves in shallow water under a non-smooth boundary with a fractal structure. The solitary wave solution was obtained using the fractal version of the variational method. Several experiments and numerical simulations have shown that disorder in nanosystems can be of fractal (self-similar) type [13–18]. In these works, the studied fractal structures were assumed to be random. In the present paper, we consider atomistic systems with deterministic quasi-fractal geometry defined below.

Recent works [3–5] have shown that molecular fractals are not exotic structures, but real systems whose geometry can be controlled. Na Li et al. [4] implemented the packing of molecular Sierpinski triangles into one-dimensional crystals. The obtained structures were studied by means of low-temperature scanning tunneling microscopy. The states described by electron wave functions of fractional dimension were observed. The wave functions delocalized over the Sierpinski structure are spread out on self-similar parts at higher energies, and this large-scale invariance can also be recovered in the reciprocal space.

We consider monolayers and nanoribbons constructed from quasi-fractal triangles. The geometry of our nanoribbons is similar to the geometry of experimental structures synthesized in [4], but we use carbon nitride triangles as structural blocks. Recently, nitrogen and carbon compounds with high N:C ratio and graphite polymer structure have been actively explored as potential next-generation materials for energy conversion and storage devices, as well as for optoelectronic and catalytic applications [19]. Among them, popular materials consist of C- and N-containing heterocycles with heptazine or triazine rings bound via sp_2-linked nitrogen atoms $N(C)_3$ or –NH– groups [19,20] (Figure 1). In some works (see, e.g., [21]), the authors consider structures where the central nitrogen atom in a heptazine triangle is substituted with a carbon atom (Figure 1c). Fractal molecular system can be obtained by creating triangular pores (by excluding the corresponding fragments), as shown in the figure. The shaded areas denote the excluded fragments to obtain a quasi-fractal monolayer of generation $g = 3$ with pores of three different sizes.

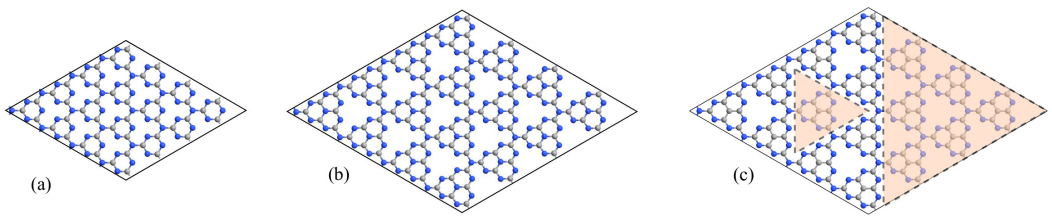

Figure 1. Triazine-based structure C_3N_4 (**a**) and poly-heptazine structure (tri-s-triazine) (**b**). Panel (**c**) shows the monolayer where the central nitrogen atom in a heptazine triangle is substituted with a carbon atom. Fractal molecular system can be obtained by creating triangular pores (by excluding the corresponding fragments), as shown in the figure. Shaded areas indicate these fragments.

In our work, quasi-fractal atomistic systems based on existing 2D materials are studied. The monolayers are subject to the DFT optimization procedure. Then, we calculate electronic properties of quasi-fractal monolayers and discuss changes of the properties with generation g of quasi-fractal blocks. Further, we construct quasi-fractal carbon nitride nanoribbons and study electron and phonon transport in a related device with attached graphene ribbons as electrodes. In the final part of the work, using the Monte Carlo simulation method, we investigate the properties of hopping transport in quasi-fractal nanoribbons and discuss the observed regimes of anomalous advection-diffusion.

2. Electronic Properties of Quasi-Fractal Carbon Nitride Monolayers

2.1. Materials and Methods

First, we consider quasi-fractal carbon nitride monolayers. These monolayers are translationally symmetric and characterized by hexagonal crystal lattice. The unit cell contains a quasi-fractal Sierpinski triangle of a certain generation g obtained by means of the procedure demonstrated in Figure 1c. We optimize the structure of these monolayers and then calculate their electronic properties. Optimization is performed by the DFT method implemented in Quantum ATK software [22]. We used the PseudoDojo pseudopotential [23] with the linear combination of atomic orbitals (LCAO) basis sets. The exchange correlation potential is described by the generalized gradient approximation (GGA) with Perdew–Burke–Ernzerhof, (PBE) functional [24]. Optimization of the structures is carried out while the atomic Hellman–Feynman force exceeded 0.01 eV/Å. Quite large vacuum region of 20 Å was used to eliminate the boundary effects. The density mesh cutoff of 105 Ha (1 Ha = 27.21 eV) was used and the $7 \times 7 \times 1$ set of k points was taken for the geometric optimization of monolayers and for calculation of their properties. The Monkhorst–Pack method [25] was used to generate k points in the Brillouin zone.

Sizes of primitive unit cells of quasi-fractal carbon nitride monolayers after optimization are listed in Table 1 for different generation g. The last column contains data on deformation ε of monolayers relative to the original 2d material ($g = 1$). As g increases, the monolayers shrink slightly. The geometry of elementary cell and the arrangement of atoms in it for four generations g are shown in Figure 2.

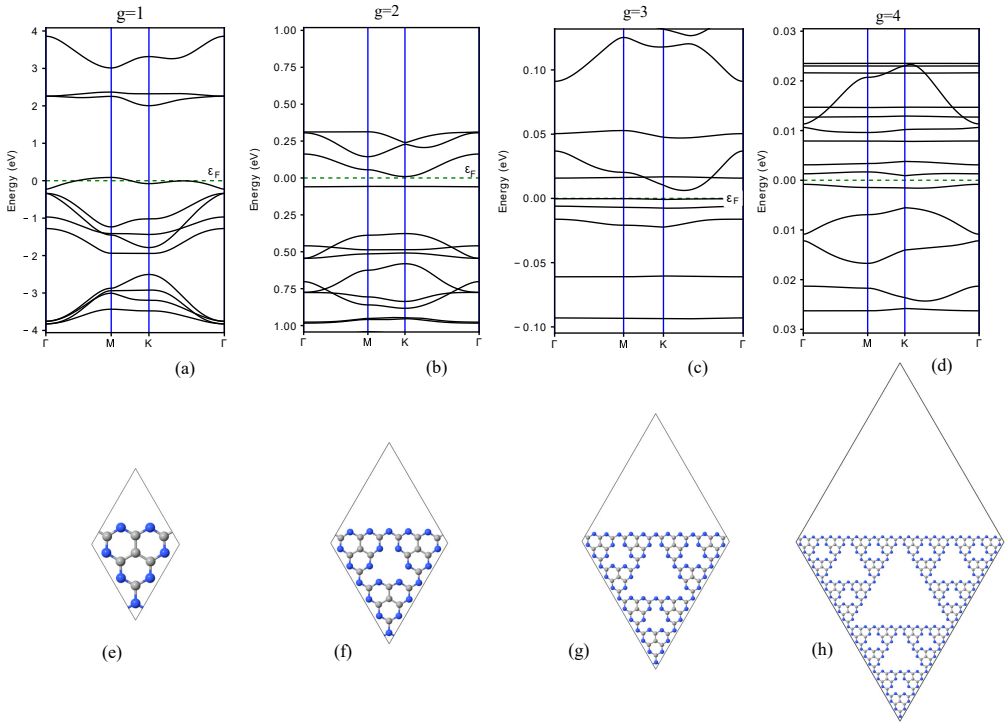

Figure 2. Band structures of quasi-fractal lattices for $g = 1$ (**a**), $g = 2$ (**b**), $g = 3$ (**c**), $g = 4$ (**d**). Corresponding primitive unit cells are shown in figures (**e**–**h**).

Table 1. Size of unit cell, bandgaps and deformation of quasi-fractal carbon nitride monolayers.

Generation	a, Å	Direct BG, meV	Indirect BG, meV	ε, %
$g = 1$	7.1316	0	0	0
$g = 2$	13.9941	66.5	66.5	−1.89
$g = 3$	27.9662	6.70	6.34	−1.96
$g = 4$	55.9194	2.12	1.73	−1.99

2.2. Band Structures

Calculated band structures for quasi-fractal carbon nitride monolayers are shown in Figure 2. Direct and indirect bandgaps are listed in Table 1. From these data, one can conclude that monolayers with $g = 2$, 3, and 4 are narrow-gap semiconductors. With the increase of g for the elementary blocks of the crystal structure, the flattening of branches is observed and, consequently, the increase in effective masses of charge carriers takes place. Individual zones for large g become simple lines of the molecular system due to the localization of charge carriers in fragments of the quasi-fractal blocks. This fact is consistent in some sense with the phenomenon of electron superlocalization [26]. Lévy and Souillard [26] showed that impurity quantum states and localized Anderson states exhibit superlocalization in fractal media, that is, their wave function decays with distance faster than exponentially. The superlocalization theory was suggested for application to amorphous or porous materials [26] with random fractal structure.

Changes in the bandstructures and density of electronic states will certainly be reflected in the modification of optical properties. Particularly, the fractal structure of mesoscopic and macroscopic electromagnetic wave receivers is often associated with the advantage of multi-band and broadband at a relatively smaller size (see, e.g., [27,28]). It is of particular interest to calculate the optical properties of atomistic quasi-fractal structures.

2.3. Absorption Spectra and Optical Conductivity

To study the absorption spectra and optical conductivity, the frequency-dependent complex dielectric function is calculated,

$$\epsilon_r(\omega) = 1 + \chi(\omega), \tag{1}$$

where ω is the photon frequency. The dielectric susceptibility $\chi(\omega)$ is calculated within the framework of the Kubo–Greenwood formalism implemented in the QuantumATK package [22]:

$$\chi_{ij}(\omega) = -\frac{e^2\hbar^4}{m^2\epsilon_0 A\omega^2}\sum_{nm}\frac{f(E_m) - f(E_n)}{E_{nm} - \hbar\omega - i\Gamma}\pi^i_{nm}\pi^j_{mn}, \tag{2}$$

where A is area, f is the Fermi–Dirac function, Γ = 0.1 eV is the broadening, π^i_{nm} is the i-th dipole matrix element between the states n and m. Local field effects are not included in the calculated permitivities and absorption spectra. The absorption coefficient is determined by the real part ϵ_1 and the imaginary part ϵ_2 of the dielectric function, and is calculated by the following formula

$$\alpha(\omega) = \sqrt{2}\frac{\omega}{c}\left(\sqrt{\epsilon_1^2(\omega) + \epsilon_2^2(\omega)} - \epsilon_1^2(\omega)\right)^{1/2}. \tag{3}$$

Optical conductivity is determined as follows

$$\sigma = -i\omega\epsilon_0\chi(\omega).$$

Figure 3 demonstrates the absorption spectra of quasi-fractal monolayers for $g = 1, 2, 3,$ and 4. As is mentioned above, fractal systems are often characterized by a wider absorption frequency range (see, e.g., [27,28]). The absorption spectra in Figure 3 indicate contrary

behavior. With increasing g, the absorption coefficient decreases, and the corresponding monolayers are characterized by narrower absorption bands. We suppose that this is related to the changes in electronic bandstructures and density of states. The spectrum of the quasi-fractal monolayers transforms from the spectrum of periodic 2d material to the spectrum of an isolated molecular system due to electron localization in quasi-fractal segments.

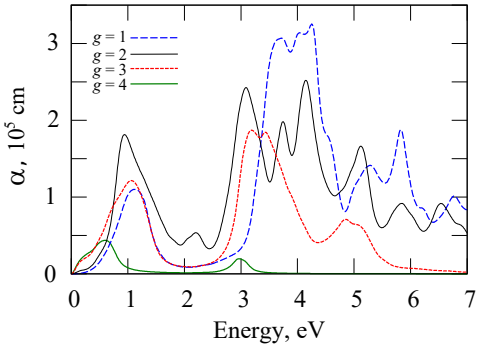

Figure 3. Absorption spectra of quasi-fractal monolayers for generations $g = 1, 2, 3$, and 4.

The enhancement of localization for larger g is also reflected in the suppression of optical conductivity. Figure 4 shows the frequency dependencies of the real and imaginary parts of the optical conductivity for the investigated quasi-fractal monolayers. As the generation g increases, the optical conductivity decreases and the nonzero conduction bands become narrower. The imaginary part of conductivity decreases as well.

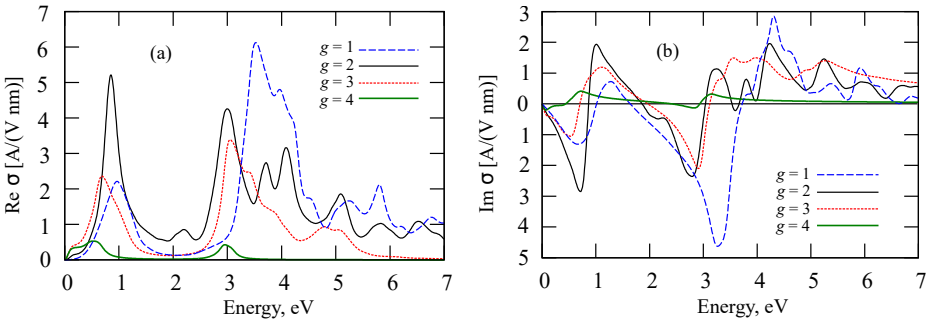

Figure 4. Real (**a**) and imaginary (**b**) parts of optical conductivity of quasi-fractal carbon nitride monolayers for $g = 1, 2, 3$, and 4.

3. Electron Transmission of Quasi-Fractal Nanoribbons

Nanoribbons or nanotubes can be obtained from the proposed quasi-fractal monolayers. In this paper, we consider nanoribbons with geometry similar to the structure of ribbons obtained experimentally in a recent work [4]. In the cited work, the authors implemented the packing of molecular Sierpinski triangles into one-dimensional crystals. The quasi-fractal blocks we use are constructed as described above from a 2D carbon nitride sheet. We attach graphene nanoribbons (nanoelectrodes) to the corners of our one-dimensional ribbons with quasi-fractal blocks to calculate electron and phonon transport, and thermolectric properties in the related devices (Figure 5). To calculate electron and phonon transmission, we use the non-equilibrium Green functions (NEGF) method implemented in QuantumATK in combination with DFT (LCAO).

The system simulating the device is divided into three regions (left electrode, central part, and right electrode). The implementation is based on the screening approximation. Within this approximation, it is assumed that the properties of the left and right electrodes are described by solving the problem for a periodic electrode cells. The approximation is valid when the current through a system is small enough that the electrodes can be characterized by an equilibrium distribution of electrons.

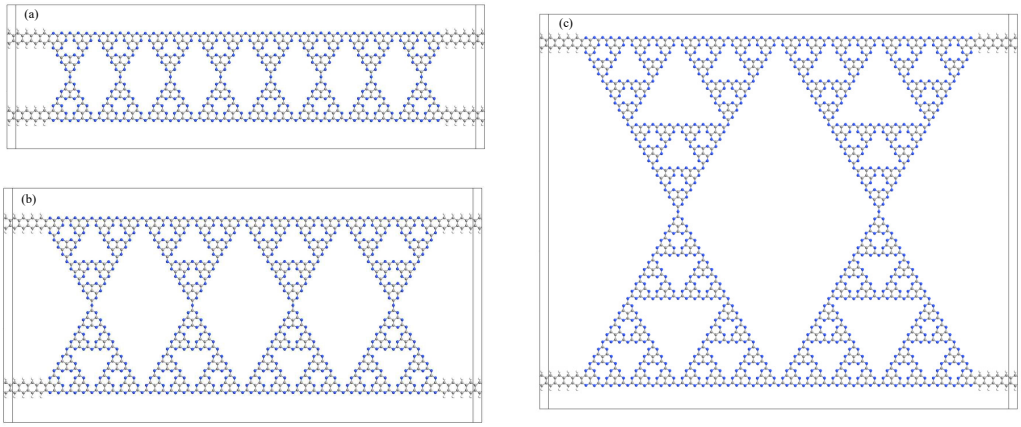

Figure 5. The geometry of devices based on carbon nitride nanoribbons with the Sierpinski triangle blocks of generation $g = 1$ (**a**), $g = 2$ (**b**), and $g = 3$ (**c**).

We calculate transmission spectra for nanoribbons with quasi-fractal blocks of three generations (see Figure 5). Nanoribbons were chosen of similar lengths (about $L = 110$ Å), but with a different number of quasi-fractal blocks. The difference in length is related to the optimization procedure performed for the blocks (see Section 2).

In QuantumATK, the transfer matrix is calculated according to the following formula

$$T_{nm}(E, \mathbf{k}) = \sum_{\ell} t_{n\ell}(E, \mathbf{k}) t^{\dagger}_{\ell m}(E, \mathbf{k}),$$

where t_{nk} is the transfer amplitude from the Bloch state ψ_n in the left electrode to the Bloch state ψ_k in the right electrode. The matrix $t^{\dagger}$ is an Hermitian conjugate. The transmittance is defined as the trace of the transmission matrix,

$$T(E, \mathbf{k}) = \sum_{n} T_{nn}(E, \mathbf{k}).$$

Let λ_α be the eigenvalues of the transfer matrix T_{nm}. From the invariance of the trace of the matrix:

$$T(E, \mathbf{k}) = \sum_{\alpha} \lambda_\alpha(E, \mathbf{k}),$$

where $\lambda_\alpha \in [0, 1]$ are transmission eigenvalues for each spin channel.

The transmission eigenstates are calculated by diagonalizing a linear combination of Bloch states, $\sum_n e_{\alpha,n}\psi_n$, where $e_{\alpha,n}$ are vectors of the basis diagonalizing the transmission matrix:

$$\sum_{m} T_{nm} e_{\alpha,m} = \lambda_\alpha e_{\alpha,n}.$$

Figure 6 presents the transmission spectra for devices based on a nitrogen–carbon quasi-fractal nanoribbon for generations $g = 1, 2$, and 3. We observe a transition from transmission bands to narrow transmission channels with increase in g. Figure 7 demonstrates examples of transmission eigenstates in quasi-fractal nitrogen–carbon nanoribbons. These states correspond to the peaks in the transmission spectra marked with points A, B, C, and D in Figure 6. The transmission eigenstates are distributed throughout the structure and take on maximum values at the edges of the quasi-fractal structure.

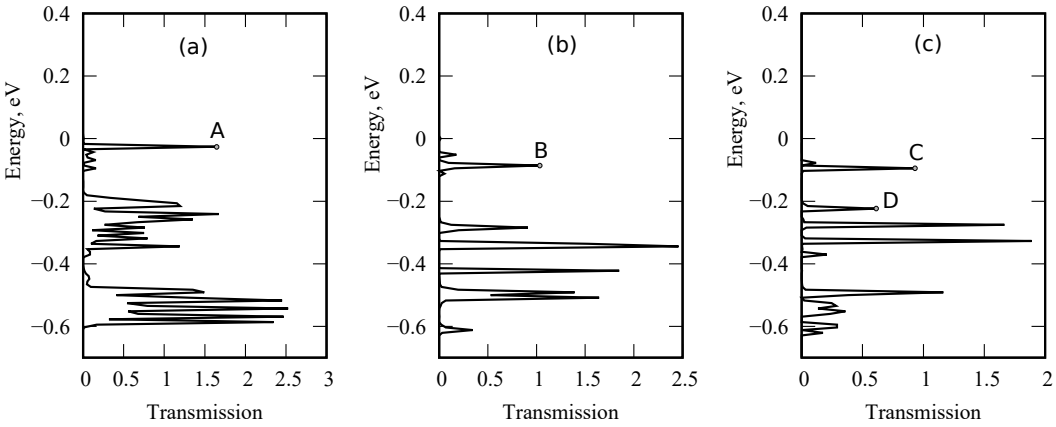

Figure 6. Transmission spectra of devices based on a nitrogen–carbon quasi-fractal nanoribbon for generations $g = 1$ (**a**), 2 (**b**), and 3 (**c**).

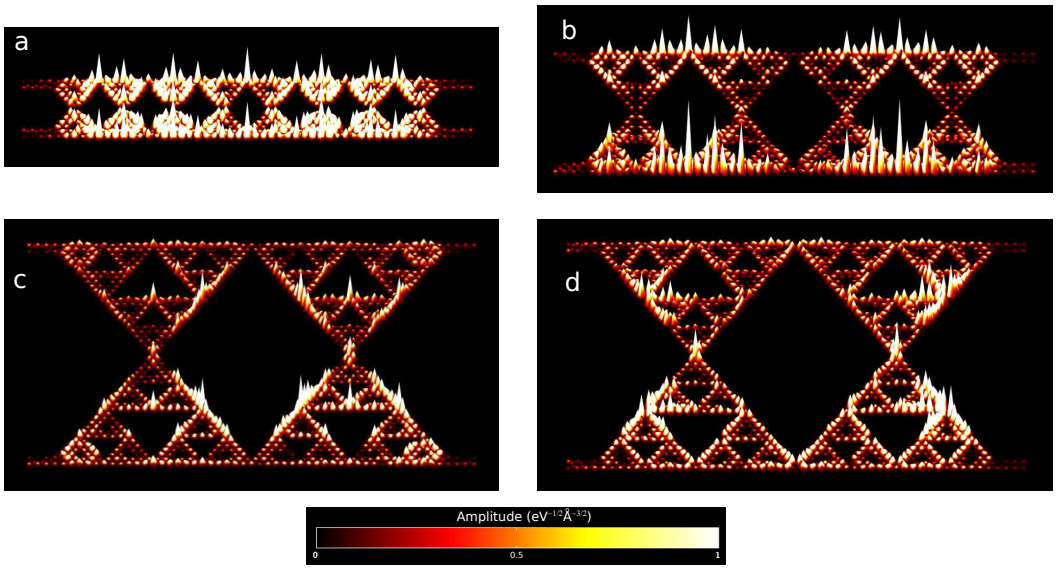

Figure 7. Visualisation of transmission eigenstates in quasi-fractal carbon nitride nanoribbons. The states correspond to points A, B, C, and D on the transmission spectra of the quasi-fractal nanoribbon for generations $g = 1$ (**a**), 2 (**b**), and 3 (**c**,**d**). All nanoribbons are located at the same angle ($\theta = 2\pi/3$). Angular inclination $\theta = 0$ corresponds to the top view, the rotation axis passes through the system center along nanoribbons. The color and height of the surface correspond to the eigenstate values in the nanoribbon plane. The color palette is the same for all pictures. Correspondence of transmission eigenstate values to a certain color is indicated on the palette scale.

4. Thermoelectric Properties

The search for new thermoelectric nanosystems is an important area of research associated with possible applications in power generation and cooling systems on nanoscales. Several studies point to the important role of quasi-one-dimensional geometry in improving the thermoelectric properties of nanosystems [29,30]. It is interesting to know how the quasi-fractal geometry of segments affects the thermoelectric characteristics. Here, we estimate thermoelectric figure of merit for quasi-fractal carbon nitride nanoribbons considered in the previous section.

The thermoelectric figure of merit ZT determines maximum efficiency of the energy conversion process in a thermoelectric material. It can be calculated by the expression

$$ZT = \frac{S^2 G T}{\lambda},$$

where S is the Seebeck coefficient, G electrical conductivity, T absolute temperature, λ thermal conductivity, which is equal to the sum of the electron λ_e and phonon λ_{ph} thermal conductivity.

The transfer coefficients were calculated using the NEGF-method, DFT, and nonequilibrium molecular dynamics. We used a model in which the central part (quasi-fractal nanoribbon) is connected to semi-infinite left and right electrodes (graphene nanoribbons). QuantumATK [22] calculates the specified thermoelectric coefficients and Peltier coefficient according to the linear response theory. The following relationships are used

$$G_{\text{e}} = \left.\frac{dI}{dV_{\text{bias}}}\right|_{dT=0}, \; S = -\left.\frac{dV_{\text{bias}}}{dT}\right|_{I=0}, \; \lambda_{\text{e}} = \left.\frac{dI_Q}{dT}\right|_{I=0}, \; \Pi = \left.\frac{I_Q}{I}\right|_{dT=0} = SV_{\text{bias}}.$$

Here $I_Q = dQ/dT$ is the electronic component of the heat flux. We use DFT method to calculate electron transmission and the molecular dynamics method to calculate phonon transmission. The optimized empirical potential ReaxFF [31] is chosen. Previously, similar computational tools have been successfully applied to a number of carbon and non-carbon nanoscale systems (see, e.g., [32–34] for details).

Figure 8 shows conductance, thermal conductivity, and thermoelectric figure of merit of devices based on nitrogen–carbon nanoribbons with molecular quasi-fractal blocks of three generations. As can be seen from the formula for ZT, an increase in the thermoelectric figure of merit can be associated, in particular, with a decrease in thermal conductivity with a slight change in electrical conduction. As the depth g of the quasi-fractal increases, the electrical conductivity and electron thermal conductivity decrease. As a result, the thermoelectric figure of merit decreases with increasing g. Thermal conductivity due to phonons does not behave monotonically with a change of g: $\lambda_{\text{ph}}(E; g = 1) < \lambda_{\text{ph}}(E; g = 3) < \lambda_{\text{ph}}(E; g = 2)$. The obtained values of the thermoelectric figure of merit are several tenths, and at some values of chemical potential are close to 1, that for some thermoelectric applications can be acceptable.

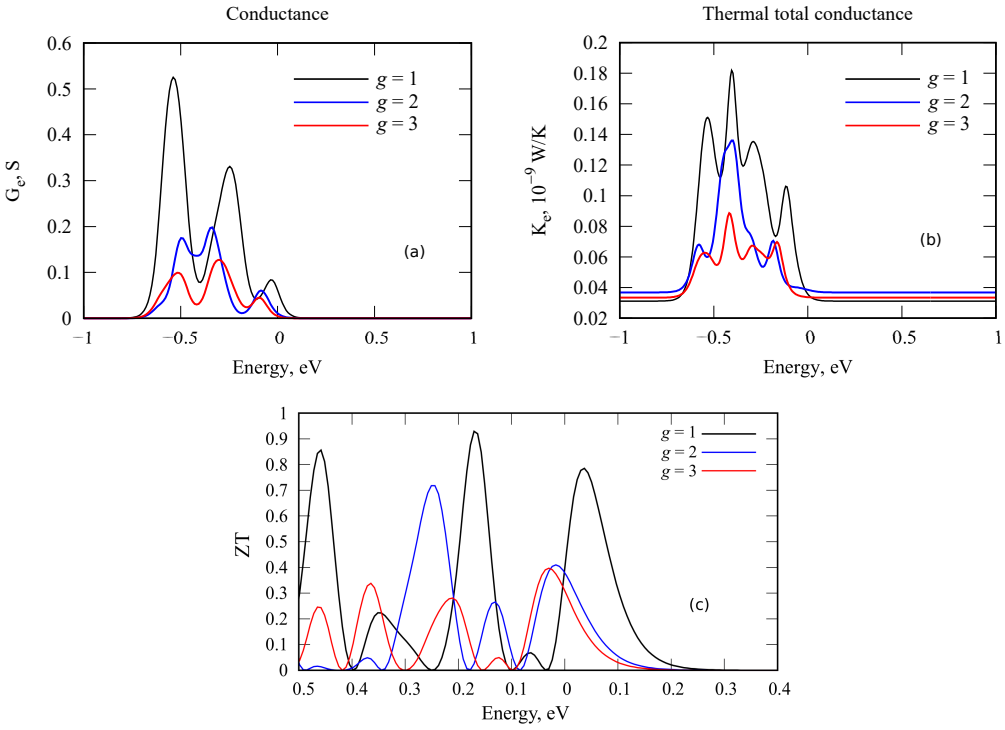

Figure 8. Conductance (**a**), thermal conductivity (**b**), and thermoelectric figure of merit (**c**) of devices based on quasi-fractal nitrogen–carbon nanoribbons.

5. Hopping in Quasi-Fractal Nanoribbons with Energetic Disorder

In this section, we introduce energetic disorder into the considered quasi-fractal nanoribbons and study hopping electron transport by Monte Carlo simulation of a biased random walk with Miller–Abrahams transfer rates. Recently, different hopping regimes have been observed in arrays of graphene quantum dots. In [35], temperature-dependent electrical measurements for graphene oxide sheets suggest that charge transport occurs via variable range hopping between intact graphene islands with sizes on the order of several nanometers. Mott variable range hopping neglects the Coulomb interaction between localized electrons in graphitic domains. At low temperatures, the Coulomb interaction should be significant and Efros–Shklovskii regime should be observed. Joung et al. [36] have shown that the low-temperature electron transport properties of chemically functionalized graphene can be explained as sequential tunneling of charges through a two-dimensional array of graphene quantum dots and resistance data exhibit Efros–Shklovskii variable range hopping arising from structural and size-induced disorder.

To perform Monte Carlo simulation of hopping between localized states, we need to define the distribution of localized states. There are two most popular forms used for disordered semiconductors. The exponential density of localized states has been substantiated for amorphous silicon, a-As_2Se_3 and some other amorphous semiconductors (see, e.g., [37]). Normal distribution is usually assumed for Gaussian disorder in organic semiconductors [38]. Lacking evidence for one of these distributions in our nanoribbons, we assume the exponential distribution of localized states

$$\rho(\varepsilon) = \rho_0 \exp(-|\varepsilon|/\varepsilon_0).$$

This distribution leads to 'heavy-tailed' distribution of waiting times and subdiffusive behavior in the dispersive transport model. In our case, the interest is related to the combined influence of the sojourn times in traps and fractal geometry. Blumen et al. [39] have shown that for particle diffusion and trapping on fractals with heavy-tailed waiting-time distributions, the mean squared displacement behaves as $\langle r^2(t)\rangle \propto t^{\alpha\beta}$, whereas the particle decay is algebraic, $S(t) \propto t^{-\alpha}$. Exponent α corresponds to power law of waiting time distribution, and β is related to walk dimension of a fractal.

Compared to the first-principles methods, the hopping model is less time-consuming for computation and allows considering deep-generation quasi-fractal systems. For our calculations, we chose ribbons with $g = 7$. In one cell, there are 10 pairs of blocks in the form of a Sierpinski triangle of generation $g = 7$. The site in our hopping model is associated with a single triangle depicted in Figure 2e. The distance between neighboring sites is estimated as a distance between central carbon atoms in neighboring triangles. This distance is equal to $d = 7.13$ Å. Localization radius and displacements are determined below in the number of these distances d. Our cell contains 10 blocks along z, each block contains $2^g = 128$ elementary triangles (sites) at the edge of a ribbon. The length of our cell is equal to $2^g \cdot 10 \cdot d = 9126.4$ Å ≈ 0.9 μm. Therefore, we consider drift and diffusion on scales from a few nanometers to micron.

Depending on the goal, different boundary conditions can be applied at the cell boundaries. To determine the time dependencies of the average position and dispersion of particle coordinate z, we use periodic boundary conditions.

In the nanoribbons under study, the transition between neighboring triangular blocks along the nanoribbon (the z axis) can occur only along the nodes located at the lateral edges of the nanoribbon. During random walk on scales much larger than the size of a single block, the diffusion of charge carriers can be approximately described by the comb model proposed in [40,41] for transport in low-dimensional percolation clusters. The diffusion equation for the case of a continuous comb structure was obtained by Arkhincheev and Baskin [42]. Its solutions, interpretation, and generalizations were considered in a number of works [43–48]. Advection-diffusion on a comb structure can be interpreted in terms of a continuous-time random walk (CTRW) model [49,50]. Diffusion in the teeth of the comb (in our case, in the blocks of nanoribbon) leads to random waiting times. Efficient transport in

the comb model is provided by transfer along the backbone. The comb model of anomalous diffusion was generalized by taking into account traps distributed over the structure [46,48], by introducing fractional Brownian motion [51], fractal geometry [45,47], multidimensional geometry [52], etc. Assuming the coexistence of two subdiffusion processes—diffusion on a fractal structure and CTRW with heavy tails, Meroz et al. [53] noticed the subordination of an ergodic anomalous process to a nonergodic one. The resulting process is non-ergodic—time-averaged and ensemble-averaged mean-square displacements do not match.

Simulating non-equilibrium hopping transport, we neglect the Coulomb interaction between localized carriers assuming small concentrations of non-equilibrium charge carriers. The probability W_{ij} to hop from an occupied site i to an empty site j with a higher energy is taken in the generalized Miller–Abrahams form

$$W_{ij} \propto= \Gamma_0 \exp\left[-2(r_{ij}/a)^{\zeta} - E_{ij}/kT\right].$$

Here, a is a localization radius, ζ is a superlocalization exponent, Γ_0 is a constant factor, kT is Boltzmann temperature, $E_{ij} = \varepsilon_i - \varepsilon_j + e\mathbf{E}\mathbf{r}_{ij}$, ε_i and ε_j energies of sites i and j, $\mathbf{r}_{ij} = \mathbf{r}_i - \mathbf{r}_j$. Related localization times are determined as

$$\tau_{i\to j} = \Gamma_0^{-1} \exp\left(\frac{\varepsilon_i - \varepsilon_j}{k_B T} + \frac{e\mathbf{E}\mathbf{r}_{ij}}{k_B T} + 2\left(\frac{r_{ij}}{a}\right)^{\zeta}\right).$$

These times are used in generation of a random waiting times set $\theta_{i\to j}$ with exponential density

$$p_{\theta_{i\to j}}(t) = \tau_{i\to j}^{-1} \exp\left(-\frac{t}{\tau_{i\to j}}\right)$$

The hop is realized to site j with minimal value of generated $\theta_{i\to j}$.

We define energies ε, ε_0, E_{ij}, $e\mathbf{E}\mathbf{r}_{ij}$ in kT units. At room temperature, 1 kT = 0.0259 eV. Electric field is defined in $kT/(ed)$ units, where $d = 7.13$ Å, and e is an electron charge. We present results for $\zeta = 1$.

Figures 9–11 show time dependencies of average coordinate $\langle z \rangle$ and centralized mean square displacement (MSD) along z-direction for different values of localization radius (Figure 9), level of disorder ε_0 (Figure 10), and different electric field (Figure 11). Parameter $\alpha = kT/\varepsilon_0$. MSD is centralized to the mean position. Displacement is measured in the amount of $d = 7.13$ Å; MSD in d^2; $\tau = \Gamma_0^{-1}$.

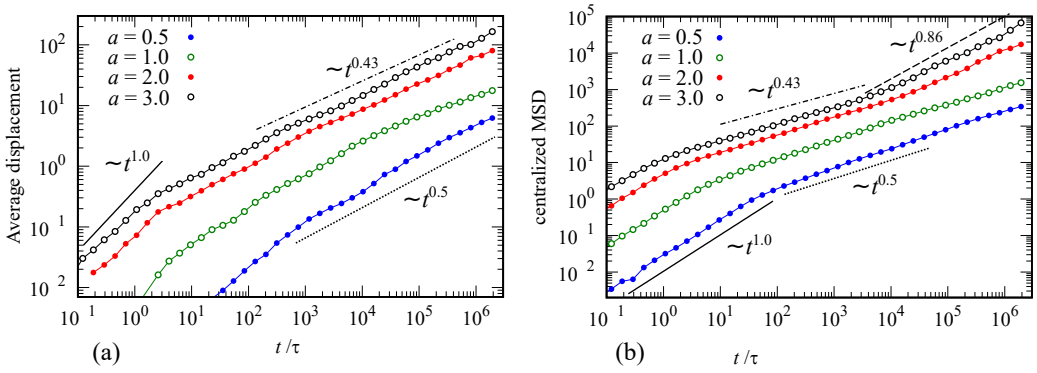

Figure 9. Average displacement (**a**) and centralized mean square displacement (MSD) (**b**) of hopping in a ribbon with Sierpinski triangle blocks for different values of localization radius. $E = 0.05\,kT/(ed)$, $\varepsilon_0 = 2\,kT$. Displacement is measured in the amount of $d = 7.13$ Å; $\tau = \Gamma_0^{-1}$.

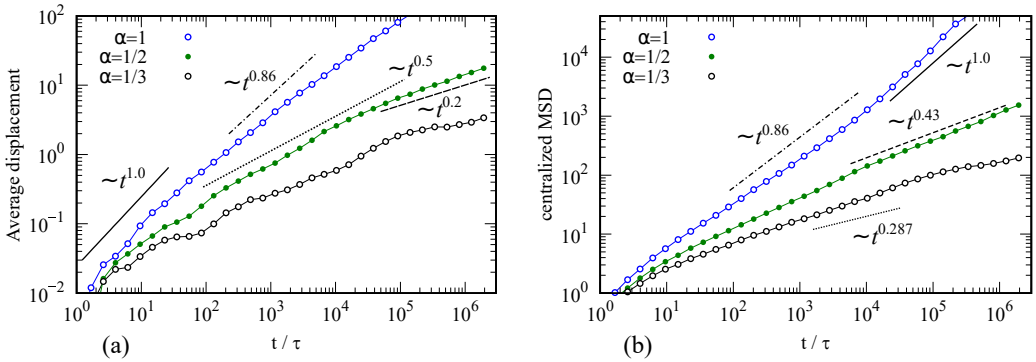

Figure 10. Average displacement (**a**) and centralized mean square displacement (MSD) (**b**) of hopping in a ribbon with Sierpinski triangle blocks for different levels of energetic disorder ε_0, $E = 0.05\, kT/(ed)$, $a = 3\, d$.

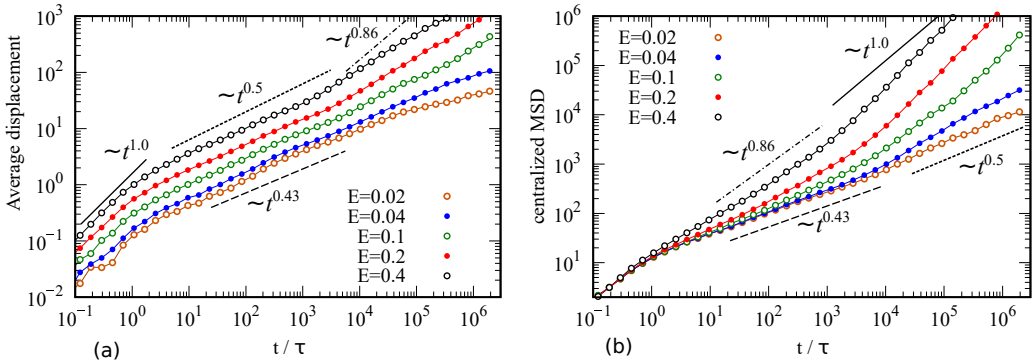

Figure 11. Average displacement (**a**) and centralized mean square displacement (MSD) (**b**) of hopping in a ribbon with Sierpinski triangle blocks for different values of external electric field E. Other parameters $\varepsilon_0 = 2\, kT$, $a = 3\, d$.

Plotting time dependencies on a double logarithmic scale, we observe power laws with different exponents for different time scales, which indicates transient anomalous diffusion. For weak electric field, the slopes of MSD in the log–log scale are almost independent of electric field. Strong electric field can change the long-time asymptotics and can lead to the superdiffusive regime (Figure 11b). The latter fact is in accordance with results presented in [54,55].

The mean square displacement for diffusion on fractal (without bias) scales with time t asymptotically as t^{2/d_w}, where the random walk dimension d_w is greater than 2 (see, e.g., [56]). For the Sierpinski triangle $d_w = \ln 5/\ln 2$, and d_w exceeds its fractal dimension $d_f = \ln 3/\ln 2$. Therefore, for simple diffusion on the Sierpinski triangle, the power law exponent for MSD vs. time is $\beta = 2/d_w \approx 0.86$. We indicate the corresponding slope in our figures. According to Blumen et al. [39], for diffusion with trapping $\langle r^2(t)\rangle \propto t^{\alpha\beta}$. In the multiple hopping model, $\alpha = kT/\varepsilon_0$. Particularly, for the case $\varepsilon_0 = 2\, kT$, product $\alpha\beta = 1/d_w = 0.43$. For reference, the corresponding power laws are shown in the figures. It should be noted that the expansion law exponent depends on the electric field, and is not determined by the simple product of α and β. The influence of energy disorder on the scaling relations under consideration depends on the localization radius a, the parameter that was absent in models of diffusion on fractals [56].

Establishing explicit dependencies of the considered scaling exponents on the parameters of hopping model requires a more systematic study involving other fractal structures. Here, we limited ourselves to the demonstration of transient anomalous diffusion for hopping in quasi-fractal nanoribbons. We observe variations of anomalous drift-diffusion parameters with localization radius, electric field intensity, and energy disorder level. The system under consideration can serve as an explicit physical implementation of the generalized comb model.

6. Conclusions

In this work, using calculations based on DFT, MD, NEGF, and Monte Carlo methods, we study electronic and phonon transport in a device based on a quasi-fractal carbon nitride nanoribbon with Sierpinski triangle blocks. The geometry of our nanoribbons is similar to the geometry of experimental structures synthesized in [4], but we use carbon nitride triangles as structural units. The monolayers and nanoribbons studied in our work are not fractals in the strict sense. The considered systems contain quasi-fractal elements constructed by the iteration method for a finite number of iterations ($g = 1, 2, 3, 4$). We calculate and analyze the change in the transport properties of nanoribbons with an increase in the generation g of quasi-fractal elements. Based on these observations, it is possible to establish a trend in the modification of these properties due to transition to a fractal structure of nanosystems.

Usually, fractal systems are characterized by a wider absorption frequency range. Contrary to this, we observe that the absorption bands are constricted for larger g and the corresponding structures are characterized by a narrower absorption range. This is due to the fact that, in comparison with macroscopic fractals, in atomistic structures, along with a change in geometry, the electronic states of the system are modified. The spectrum of the quasi-fractal system under consideration tends to range from the spectrum of the periodic 2d system to the spectrum of an isolated molecular system.

The obtained values of the thermoelectric figure of merit are several tenths, and at some values of the energy are close to 1, which indicates the possible use of the considered nanoribbons for thermoelectric applications, although it should be noted that with an increase in g, the characteristic values of ZT decrease.

Using the Monte Carlo technique and the Miller–Abrahams relation for transfer rates, we simulate hopping transport of charge carriers in quasi-fractal nanoribbons. Variations of anomalous drift-diffusion parameters with localization radius, temperature, electric field intensity, and energy disorder level are studied. It should be noted that the expansion law exponent depends on the electric field, and is not determined by the simple product of α and β. The influence of energy disorder on the time scaling of mean square displacement depends on the localization radius a, the parameter that was absent in models of diffusion on fractals. These nanoribbons can be considered as an explicit physical implementation of the comb model.

Author Contributions: Conceptualization, R.T.S. and A.K.G.; Data curation, E.V.M. and D.A.T.; Formal analysis, R.M.M., E.V.M. and D.A.T.; Investigation, A.K.G.; Methodology, R.T.S. and A.K.G.; Software, R.M.M., E.V.M. and D.A.T.; Writing—original draft, R.T.S.; Writing—review & editing, R.M.M. All authors have read and agreed to the published version of the manuscript.

Funding: The work is partially supported by the Ministry of Science and Higher Education of the Russian Federation (project FNRM-2021-0002).

Institutional Review Board Statement: Not applicable.

Informed Consent Statement: Not applicable.

Acknowledgments: We thank anonymous reviewers for many insightful comments and suggestions.

Conflicts of Interest: The authors declare no conflict of interest.

References

1. Haldane, F. D. M. 'Luttinger liquid theory' of one-dimensional quantum fluids. I. Properties of the Luttinger model and their extension to the general 1D interacting spinless Fermi gas. *J. Phys. C Solid State Phys.* **1981**, *14*, 2585. [CrossRef]
2. Zhang, Y.; Yan-Wen, T.; Horst L, S.; Kim, P. Experimental observation of the quantum hall effect and Berry's phase in graphene. *Nature* **2005**, *438*, 201–204. [CrossRef] [PubMed]
3. Kempkes, S.; Slot, M.; Freeney, S.; Zevenhuizen, S.; Vanmaekelbergh, D.; Swart, I.; Smith, M. Design and characterization of electrons in a fractal geometry. *Nat. Phys.* **2019**, *15*, 127–131. [CrossRef] [PubMed]
4. Li, N.; Gu, G.; Zhang, X.; Song, D.; Zhang, Y.; Teo, B.K.; Peng, L.; Hou, S.; Wang, Y. Packing fractal Sierpiński triangles into one-dimensional crystals via a templating method. *Chem. Commun.* **2017**, *53*, 3469–3472. [CrossRef]

5. Li, C.; Zhang, X.;Li, N.; Wang, Y.; Yang, J.; Gu, G.; Zhang, Y.; Hou, S.; Peng, L.; Wu, K.; et al. Construction of Sierpinski triangles up to the fifth order. *J. Am. Chem. Soc.* **2017**, *139*, 13749–13753 [CrossRef]
6. Ghadiyali, M.; Chacko, S. Confinement of wave-function in fractal geometry, a detection using DFT. *arXiv* **2019**, arXiv:1904.11862.
7. Westerhout, T.; van Veen, E.; Katsnelson, M.I.; Yuan, S. Plasmon confinement in fractal quantum systems. *Phys. Rev. B* **2018**, *97*, 205434. [CrossRef]
8. Pedersen, T.G. Graphene fractals: Energy gap and spin polarization. *Phys. Rev. B* **2020**, *101*, 235427. [CrossRef]
9. Khalili Golmankhaneh, A.; Kamal Ali, A. Fractal Kronig-Penney model involving fractal comb potential. *J. Math. Model.* **2021**, *9*, 331–345.
10. Xu, X.Y.; Wang, X.W.; Chen, D.Y.; Smith, S.M.; Jin, X.M. Quantum transport in fractal networks. *Nat. Photonics* **2021**, *15*, 703–710. [CrossRef]
11. Zosimov, V. V.; Lyamshev, L. M. Fractals in wave processes. *Physics-Uspekhi* **1995**, *38*, 347. [CrossRef]
12. Wang, K. J.; Li, G.; Liu, J. H.; Wang, G. D. Solitary waves of the fractal regularized long-wave equation traveling along an unsmooth boundary. *Fractals* **2021**, *2021*, 2250008. [CrossRef]
13. Pook, W.; Janßen, M. Multifractality and scaling in disordered mesoscopic systems. *Z. Phys. B Condens. Matter* **1991**, *82*, 295–298. [CrossRef]
14. Hegger, H.; Huckestein, B.; Hecker, K.; Janssen, M.; Freimuth, A.; Reckziegel, G.; Tuzinski, R. Fractal conductance fluctuations in gold nanowires. *Phys. Rev. Lett.* **1996**, *77*, 3885. [CrossRef]
15. Barthelemy, P.; Bertolotti, J.; Wiersma, D.S. A Lévy flight for light. *Nature* **2008**, *453*, 495. [CrossRef]
16. Kohno, H.; Yoshida, H. Multiscaling in semiconductor nanowire growth. *Phys. Rev. E* **2004**, *70*, 062601. [CrossRef]
17. Kohno, H. Self-organized nanowire formation of Si-based materials. In *One-Dimensional Nanostructures*; Springer: Berlin/Heidelberg, Germany, 2008; pp. 61–78.
18. Raboutou, A.; Peyral, P.; Lebeau, C.; Rosenblatt, J.; Burin, J.P.; Fouad, Y. Fractal vortices in disordered superconductors. *Phys. A Stat. Mech. Its Appl.* **1994**, *207*, 271–279. [CrossRef]
19. Miller, T.S.; Jorge, A.B.; Suter, T.M.; Sella, A.; Corà, F.; McMillan, P.F. Carbon nitrides: Synthesis and characterization of a new class of functional materials. *Phys. Chem. Chem. Phys.* **2007**, *19*, 15613–15638. [CrossRef]
20. Bafekry, A.; Shayesteh, S.F.; Peeters, F.M. Two-dimensional carbon nitride (2d-CN) nanosheets: Tuning of novel electronic and magnetic properties by hydrogenation, atom substitution and defect engineering. *J. Appl. Phys.* **2019**, *126*, 215104. [CrossRef]
21. Bafekry, A.; Faraji, M.; Karbasizadeh, S.; Hieu, N.N.; Ang, Y.S.; Sarsari, I.A.; Ghergherehchi, M. Two-dimensional dirac half-metal in porous carbon nitride C6N7 monolayer via atomic doping. *Nanotechnology* **2021**, *33*, 075707. [CrossRef]
22. Smidstrup, S.; Markussen, T.; Vancraeyveld, P.; Wellendorff, J.; Schneider, J.; Gunst, T.; Verstichel, B.; Stradi, D.; Khomyakov, P.A.; Vej-Hansen, U. G.; et al. QuantumATK: An integrated platform of electronic and atomic-scale modelling tools. *J. Phys. Condens. Matter* **2019**, *32*, 015901. [CrossRef] [PubMed]
23. Van Setten, M. J.; Giantomassi, M.; Bousquet, E.; Verstraete, M. J.; Hamann, D. R.; Gonze, X.; Rignanese, G. M. The PseudoDojo: Training and grading a 85 element optimized norm-conserving pseudopotential table. *Comput. Phys. Commun.* **2018**, *226*, 39–54. [CrossRef]
24. Perdew, J. P.; Burke, K.; Ernzerhof, M. Generalized gradient approximation made simple. *Phys. Rev. Lett.* **1996**, *77*, 3865. [CrossRef]
25. Monkhorst, H. J.; Pack, J. D. Special points for Brillouin-zone integrations. *Phys. Rev. B* **1976**, *13*, 5188. [CrossRef]
26. Levy, Y. E.; Souillard, B. Superlocalization of electrons and waves in fractal media. *EPL (Europhys. Lett.)* **1987**, *4*, 233. [CrossRef]
27. Choukiker, Y. K.; Behera, S. K. Modified Sierpinski square fractal antenna covering ultra-wide band application with band notch characteristics. *IET Microwaves Antennas Propag.* **2014**, *8*, 506–512. [CrossRef]
28. Darimireddy, N. K.; Reddy, R. R.; Prasad, A. M. A miniaturized hexagonal-triangular fractal antenna for wide-band applications. *IEEE Antennas Propag. Mag.* **2018**, *60*, 104–110. [CrossRef]
29. Ouyang, Y.; Guo, J. A theoretical study on thermoelectric properties of graphene nanoribbons. *Appl. Phys. Lett.* **2009**, *94*, 263107. [CrossRef]
30. Kodama, T.; Ohnishi, M.; Park, W.; Shiga, T.; Park, J.; Shimada, T.; Shinohara, H.; Shiomi, J.; Goodson, K.E. Modulation of thermal and thermoelectric transport in individual carbon nanotubes by fullerene encapsulation. *Nat. Mater.* **2017**, *16*, 892–897. [CrossRef]
31. Pai, S.J.; Yeo, B.C.; Han, S.S. Development of the reaxff cbn reactive force field for the improved design of liquid CBN hydrogen storage materials. *Phys. Chem. Chem. Phys.* **2016**, *18*, 1818–1827. [CrossRef]
32. Markussen, T.; Jauho, A.P.; Brandbyge, M. Electron and phonon transport in silicon nanowires: Atomistic approach to thermoelectric properties. *Phys. Rev. B* **2009**, *79*, 035415. [CrossRef]
33. Meftakhutdinov, R. M.; Sibatov, R. T.; Kochaev, A. I. Graphenylene nanoribbons: Electronic, optical and thermoelectric properties from first-principles calculations. *J. Phys. Condens. Matter* **2020**, *32*, 345301. [CrossRef] [PubMed]
34. Kochaev, A. I.; Meftakhutdinov, R. M.; Sibatov, R. T.; Timkaeva, D. A. Optical and thermoelectric properties of graphenylene and octagraphene nanotubes from first-principles calculations. *Comput. Mater. Sci.* **2021**, *186*, 109999. [CrossRef]
35. Gómez-Navarro, C.; Weitz, R.T.; Bittner, A.M.; Scolari, M.; Mews, A.; Burghard, M.; Kern, K. Electronic transport properties of individual chemically reduced graphene oxide sheets. *Nano Lett.* **2007**, *7*, 3499–3503. [CrossRef]
36. Joung, D.; Zhai, L.; Khondaker, S.I. Coulomb blockade and hopping conduction in graphene quantum dots array. *Phys. Rev. B* **2011**, *83*, 115323. [CrossRef]
37. Pfister, G.; Scher, H. Dispersive (non-Gaussian) transient transport in disordered solids. *Adv. Phys.* **1978**, *27*, 747–798. [CrossRef]

38. Bässler, H. Charge transport in disordered organic photoconductors. A Monte Carlo simulation study. *Phys. Status Solidi (Basic Res.)* **1993**, *175*, 15–56. [CrossRef]
39. Blumen, A.; Klafter, J.; White, B.S.; Zumofen, G. Continuous-time random walks on fractals. *Phys. Rev. Lett.* **1984**, *53*, 1301. [CrossRef]
40. White, S.R.; Barma, M. Field-induced drift and trapping in percolation networks. *J. Phys. A Math. Gen.* **1984**, *17*, 2995–3008. [CrossRef]
41. Weiss, G.H.; Havlin, S. Some properties of a random walk on a comb structure. *Phys. A Stat. Mech. Appl.* **1986**, *134*, 474–482. [CrossRef]
42. Arkhincheev, V.E.; Baskin, E.M. Anomalous diffusion and drift in a comb model of percolation clusters. *Sov. Phys. JETP* **1991**, *73*, 161–165.
43. Baskin, E.; Iomin, A. Superdiffusion on a comb structure. *Phys. Rev. Lett.* **2004**, *93*, 120603. [CrossRef]
44. Lubashevskii, I.A.; Zemlyanov, A.A. Continuum description of anomalous diffusion on a comb structure. *J. Exp. Theor. Phys.* **1998**, *87*, 700–713. [CrossRef]
45. Iomin, A. Subdiffusion on a fractal comb. *Phys. Rev. E* **2011**, *83*, 052106. [CrossRef]
46. Sibatov, R.T.; Morozova, E.V. Multiple trapping on a comb structure as a model of electron transport in disordered nanostructured semiconductors. *J. Exp. Theor. Phys.* **2015**, *120*, 860–870. [CrossRef]
47. Sandev, T.; Iomin, A.; Méndez, V. Lévy processes on a generalized fractal comb. *J. Phys. A Math. Theo.* **2016**, *49*, 355001. [CrossRef]
48. Sandev, T.; Iomin, A.; Kantz, H.; Metzler, R.; Chechkin, A. Comb model with slow and ultraslow diffusion. *Math. Model. Nat. Phenom.* **2016**, *11*, 18–33. [CrossRef]
49. Metzler, R.; Klafter, J. The random walk's guide to anomalous diffusion: A fractional dynamics approach. *Phys. Rep.* **2000**, *339*, 1–77. [CrossRef]
50. Sokolov, I.M. Models of anomalous diffusion in crowded environments. *Soft Matter* **2012**, *8*, 9043–9052. [CrossRef]
51. Zahran, M.A.; Abulwafa, E.M.; Elwakil, S.A. The fractional Fokker-Planck equation on comb-like model. *Phys. A Stat. Mech. Appl.* **2003**, *323*, 237–248. [CrossRef]
52. Arkhincheev, V.E. Unified continuum description for sub-diffusion random walks on multi-dimensional comb model. *Phys. A Stat. Mech. Appl.* **2010**, *389*, 1–6. [CrossRef]
53. Meroz, Y.; Sokolov, I.M.; Klafter, J. Subdiffusion of mixed origins: When ergodicity and nonergodicity coexist. *Phys. Rev. E* **2010**, *81*, 010101. [CrossRef]
54. Hou, R.; Cherstvy, A.G.; Metzler, R.; Akimoto, T. Biased continuous-time random walks for ordinary and equilibrium cases: Facilitation of diffusion, ergodicity breaking and ageing. *Phys. Chem. Chem. Phys.* **2018**, *20*, 20827–20848. [CrossRef]
55. Wang, W.; Barkai, E. Fractional advection-diffusion-asymmetry equation. *Phys. Rev. Lett.* **2020**, *125*, 240606. [CrossRef]
56. Ben-Avraham, D.; Havlin, S. *Diffusion and Reactions in Fractals and Disordered Systems*; Cambridge University Press: Cambridge, UK, 2000.